



REGULAR PAPER

Effects of blowing upon dynamic stability of blunt nosed re entry vehicles pitching in hypersonic flow

M. Khalid  and K.A. Juhany 

Department of Aerospace Engineering, King Abdul Aziz University, Jeddah, Saudi Arabia

Corresponding author: M. Khalid; Email: mkholid@kau.edu.sa

Received: 4 November 2022; Revised: 18 July 2023; Accepted: 20 July 2023

Keywords: hypersonic dynamic stability; bluntness effects; blowing effects; carbuncle phenomenon; strong shock effects; frontal and tangential blowing

Abstract

Blowing is often used to alleviate the intense heating rates on blunt noses of hypersonic vehicles. This flow efflux at the leading edge transforms the flow field in the blunt-nose regions with implications on the dynamic stability of the vehicles. As a demonstrative exercise, the flow fields past blunt-nosed and truncated-nosed conical bodies under blowing and no-blowing conditions were perturbed to obtain the unsteady effects using the shock expansion method to recover the unsteady pressure coefficient. Static and pitching moment derivatives were then duly obtained by integrating the differential of the unsteady pressure coefficient with respect to the pitch angle (α) or the pitch rate ($\dot{\theta}$) together with the moment arm with reference to the centre of gravity. The results obtained for blunt-nose and truncated conical bodies show a noticeable drop in dynamic stability. Even when the flow is transformed from a tangential blowing at the shoulder of the blunt-nosed vehicle shows some degradation in dynamic stability.

Nomenclature

α	Angle-of-attack
c	body length
Cp	pressure coefficient $\frac{2}{\gamma M_\infty^2} \left\{ \frac{p}{p_\infty} - 1 \right\}$
Cm_q	$\frac{2V_\infty}{c} \frac{\partial Cm}{\partial q}$
Cm_α	$\frac{V_\infty}{c} \frac{\partial Cm}{\partial \alpha}$
$h(x,t)$	instantaneous height of a point on the body
l	Moment arm
ρ	Fluid density
p	Pressure
$P_{b,s}$	Pressure with blowing or on solid surface
$p'_{b,s}$	Pressure perturbation due to unsteadiness
P_{ref}	Pressure at the reference location
P_∞	Free stream pressure
R_B	Base radius
R_N	Nose radius
S	Reference area
T	Temperature
X	Axial distance
V	Velocity magnitude
$R(x)$	Local radius

Re	Reynolds number
M	Mach number
M_x	Local Mach number
q	<i>pitch rate</i>
t	time for particle to move from apex to station x
$\Delta\varepsilon_p(x)$	change in angle of inclination of tangent to (projected) streamline (path line) of a particular fluid element between vertex and point $(x, R(x), \varphi)$ on body surface, measured in osculating plane of reference
$\theta_b(x)$	local angle of inclination of body surface to axis of symmetry
θ_0	slope of the body at the designated apex
ϑ	pitch angle
φ	azimuthal direction ($360-\theta$) measured clockwise from the starboard radius on the horizontal diameter plane through the vertex

1.0 Introduction

Dynamic stability for vehicles pitching or plunging in hypersonic flow has been studied at length both experimentally and analytically. Dynamic stability at hypersonic Mach numbers is difficult to resolve as the disturbances that influence unsteady aerodynamic loads promoting high-frequency model oscillations are difficult to model. Accounting for the effect of these small-scale disturbances in experiments or through numerical resolution is difficult and times consuming, respectively. In wind tunnel experiments, the model mounted on a cross flexure or held about a typical CG location in a magnetic field is subjected to oscillations under wind-off and wind on hypersonic flow conditions. In more sophisticated free range facilities, the model is literally fired in between two stations up to 100 m apart. The frequency of oscillations trace and the decay in oscillation amplitude trace under wind-on and wind off conditions along with the spring constant readily provides the static (C_{m_α}) and dynamic moment coefficients ($C_{m_\dot{\theta}}$). The challenge in the experimental method using short duration facilities is being able to maintain uniform hypersonic flow to obtain at least 10–15 complete oscillation cycles to ascertain accurate and adequate amplitude decay and frequency determination. On the other hand, larger industrial level hypersonic facilities can readily provide the uniform flow for sufficiently long run times to comfortably recover dynamic stability characteristics.

For numerical simulation using CFD techniques, the unsteady flow field past a blunt model executing high-frequency oscillation would be extremely difficult and expensive to resolve. The viscous flow field near the blunt nose would be even more difficult to resolve for an unsteady oscillating model. The use of LES or DNS would put it beyond the reach of most universities as the mesh requirements and other costs related to extensive computational times would be absolutely prohibitive. The iterative computational time step would have to be a very small, as the high-frequency motion would dictate a very small periodic time for a complete cycle necessitating an enormous number of individual time steps at which the required level of density or other lux residual levels are adequately satisfied. One of the first numerical modeling was carried out by Rie et al. [1].

Tracking the progress in this discipline, there were important AGARD Refs [2, 3], which took a comprehensive stock of the dynamic stability parameters from all experimental and numerical sources. Other important individual contributions have been itemised by Khalid [4, 5] in some earlier publications. Beyond solid body dynamic stability investigation for sharp- or blunt-nosed configurations, there have been little effort in recovering static or dynamic moment derivatives when the blowing is turned on at the nose to alleviate any heating effects. For experimental studies, such mechanisms would be difficult to install around the blunt nose, where the flow ejection rates from the solid surface in the local region would have to be higher than the on-coming flow velocities in order to make a noticeable difference to the heating flux. For the numerical studies, even under steady flow conditions it was found that the interaction between the on-coming flow and the strong efflux from the nose leads to complex flow instabilities known as the carbuncle flow phenomenon. The flow field continues to show signs of convergence

followed by instantaneous breakdown of flow convergence before it begins to converge again. This complexity is only a small part of the problems experienced when simulating unsteady viscous hypersonic flows.

The present work makes use of the more exactly flow field past the blunt models equipped with the blowing near the nose switched on to minimise the heating effects. Dynamic stability for blunt hypersonic vehicles with blowing has not been investigated in any depth in the past. Computation of flow field past blunt axi-symmetric bodies is difficult owing to strong shock effects and complexity of flow in the blunt-nose region where the flow passes through subsonic to sonic to hypersonic flow regimes in a very small region of the flow. When the flow is equipped with surface blowing out of the blunt surface it exacerbates the flow further as the efflux boundary condition is difficult to apply invariably leading to solution breakdown as the solution becomes instable as the physics transforms instantly. It is a non-trivial exercise to successfully recover the steady pressure flow field on a body with efflux and pitching in hypersonic flow field. The resulting steady pressure field is then perturbed using the shock expansion to account for the unsteady effects instead of actually computing the complex and costly unsteady flow field. The effects of immediate angle-of-attack is duly built into the analytic expression before obtaining the appropriate static and dynamic moment coefficients, which are in turn integrated over the surface of the complete model to obtain the dynamic stability characteristics.

In all, four blunt models were investigated, which included two blunt cones of bluntness (R_N/R_B) 0.34 and 0.12 with a half-angle of 12.5° , as well as a truncated model flat sharp nosed model having a circular front nose to base diameter ratio of 0.11. In order to assess the effects of tangential blowing as separate from the previous frontal blowing, a round-nosed model of bluntness 0.34 was also investigated. In each case, the results from a corresponding solid model were also computed to identify the isolate the effects of blowing. The steady state results obtained from the computational study were duly compared to the experiment as reported by Nowak [6]. The results reported by Nowak were directly related to the pure cones studies in this paper. Elsewhere, there have been other more recent flow field studies on non-pure cones carried out by Tissera et al. [7] to obtain pressure distribution and heat transfer rates on HB-2 configurations. This study made successful use of the Harten-Lax van Leer contact Riemann solver in conjunction with fifth and ninth order WENO-M schemes as well as the second order MUSCLE scheme. Paranas and Drikakis [8] have also numerically simulated unsteady flows at high Mach numbers around spiked blunt bodies. The experimental studies as reported by Paranas and Drikakis were also carried out to know the effect of variations to the spike diameter to blunt body. Along similar vein the work by Narayan et al. [9] numerically and experimentally investigates the flow at $M = 5.8$ flow past varying nose cone configurations such as taper/stepped taper spiked, spherically blunted, and parabolic nose cones at a fineness ratio of 3.6 and $\alpha = 0$, in order to determine the best passively modified geometry that provides the control of both the aerodynamic drag coefficient and surface heat flux. Another important by Wantabe et al. [10] study involves investigating the flow field by allowing the air at $M = 7$ to enter the stagnation region at the blunt nose and ejected at the base. The alleviation of pressure at the nose and suction at the nose should allegedly lead to at least 5% drag reduction.

Other than the Newak [6] work dealing with simple conical shapes, most of the above cases deal with spiked models or the HP-2 configurations. Steady pressure distributions were suitably perturbed using the shock expansion technique and the deflection of the surface streamlines as the underlying body oscillates. It was learnt in all cases that blowing leads to deterioration in dynamic stability performance. A parallel observation for dynamic stability of blunt cones was that using classic universal curve for steady pressure field indiscriminately for blunt cones of any bluntness may lead to erroneous result.

2.0 Computational approach to steady flow field with and without frontal blowing

The conservative form of the compressible Reynolds-Averaged Navier-Stokes equations as used in the algorithm is as follows:

$$\frac{\partial \rho}{\partial t} + \frac{\partial [\rho u_j]}{\partial x_j} = 0 \tag{1}$$

$$\frac{\partial}{\partial t} (\rho u_i) + \frac{\partial}{\partial x_j} \left[\rho u_i u_j + p \delta_{ij} - \left(1 + \frac{\mu_t}{\mu} \right) \tau_{ij} \right] = 0 \tag{2}$$

$$\frac{\partial}{\partial t} (\rho E) + \frac{\partial}{\partial x_j} \left[\rho u_j E + u_j p - \left(1 + \frac{\mu_t}{\mu} \right) u_i \tau_{ij} - \left(c_p \frac{\mu}{Pr} + c_p \frac{\mu_t}{Pr_t} \right) \frac{\partial T}{\partial x_j} \right] = 0 \tag{3}$$

ρ in these equations refers to the density, p the pressure and T is the temperature. E is the total energy and u is the velocity vector in tensor format. τ_{ij} is the viscous stress tensor which may be written as:

$$\tau_{ij} = \mu \left(\frac{\partial u_i}{\partial x_j} + \frac{\partial u_j}{\partial x_i} - \frac{2}{3} \frac{\partial u_k}{\partial x_k} \delta_{ij} \right) \tag{4}$$

The above Navier Stokes equations, formulated in strong conservation form to be used in the structured meshes of the present study, are first cast into curvilinear coordinate scheme following Vinokur [11] transformation method. The numerical algorithm used to solve the Navier Stokes equations is an implicit factorisation finite centre difference scheme about a regular rectangular prism, which is described at length by Beam and Warming [12]. Local time linearisation is applied to the non-linear terms following Pulliam and Chausee [13]. Approximate factorisation scheme is applied to the resulting matrices, which factorises the operator itself resulting in efficient matrix equations with narrow bandwidth. This results in block tridiagonal matrices, which are easy to solve. The spatial derivatives can thus be approximated using second order central differences. Explicit and implicit artificial dissipation terms are added to achieve nonlinear stability. A spatially variable time step is used to accelerate convergence to steady state solutions. The algorithm can be used to solve time accurate or steady state flow problems.

The fact that the Navier Stokes equations are formulated in a strong conservation form as well as the implicit treatment of the artificial dissipation and the inclusion of a second order dissipation terms helps in the shock capturing at high Mach numbers.

We selected k- ϵ and the Wilcox k- ω turbulence models for this investigation. For the two equations turbulence models, the convection and diffusion terms of their transport equations are negligible in the inertial sublayer so that local equilibrium prevails, which implies that the production of the turbulent kinetic energy k is equal to the dissipation rate. The local equilibrium condition leads to two simple relations that can be used as boundary conditions for k and the dissipation terms for both incompressible and compressible flows. The compressible wall functions have been successfully applied to both attached and separated flows under Mach number ranging from 0.1 to 10.

While the purpose in this study was not to scrutinise the capabilities of the turbulence models, nevertheless for these simple bodies, very little difference in results was observed from the two turbulence models. The Sutherland law is implemented to compute the laminar viscosity coefficient (μ). Since the flows computed involve hypersonic Mach number the choice of the Prandtl number is selected to suite the Mach number whereas the use of specific heat and the specific heat ratio c_p/c_v (γ) in the algorithm for one species gas must also respect the high Mach number flow conditions subject to the relations by Grundmann [14] and Gordon and McBride [15]:

$$c_v(T) = R \left(\frac{5}{2} + \frac{\left(\frac{hv^2}{kT} \right) e^{hv/kT}}{\left(e^{kT} - 1 \right)^2} \right), \quad c_p(T) - c_v(T) = R$$

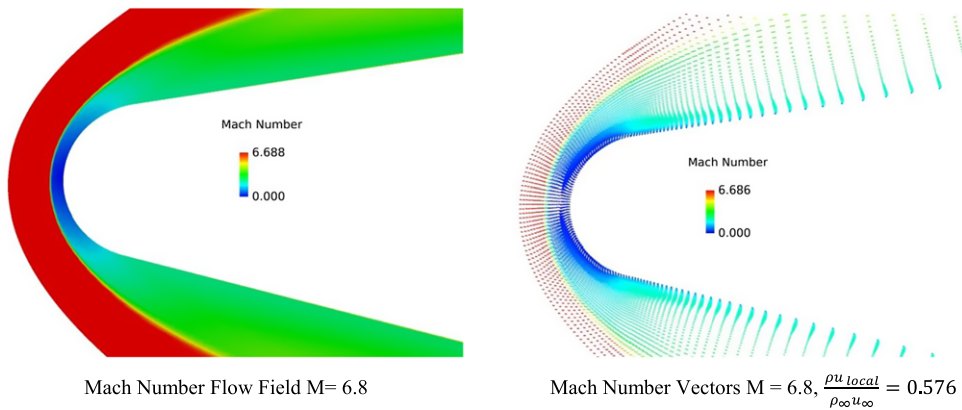


Figure 1. Mach number (solid surface) and velocity vectors (with frontal blowing) past a blunt cone of bluntness 0.32.

$$\frac{c_p(T)}{R} = \sum_{n=0}^{n=4} a_n T^n \tag{5}$$

Where T is temperature, R is the real gas constant, h is Planck’s constant, ν is the fundamental vibrational frequency and k is Boltzman’s constant, and where a_n are curve-fit constants. As explained in Khalid and Juhany [16] the input flow conditions (ρ , ρu_i , E) for the outflow surface are treated like a new ‘slip’ condition, which remains fixed during the flow applied run. The algorithm iterates between the successive grid planes near the exit control boundary until the desired flow conditions are matched at the exit boundary as the convergence criterion is reached. For the corresponding solid surface run this surface would understandably carry a no-slip boundary condition. Since the present applications of the code deals with axi-symmetric flow fields produced when a simple two-dimensional mesh is rotated about the body axis through a 45° azimuthal angle. The flow has to be carefully treated near the polar stations. In such cases a computational coordinate surface may represent a physical 3D line. For example, with an “O” grid the circles (2D) or cylinders (3D) collapse to points and lines, respectively. The flow variables at the singular boundary are the average of the points surrounding the singular point.

The flow field as recovered from using above CFD method on a solid blunt cone of bluntness 0.34 and the same body with frontal blowing rate of $\frac{\rho u_{local}}{\rho_{\infty} u_{\infty}} = 0.576$ are shown in Fig. 1. The outflow at the leading edge was only implemented around the front blunt nose. Following the hypersonic heat alleviation experiment [6], the efflux rate here corresponds to mass rate of 2.09 kg/s. A similar study was conducted on a blunt cone of bluntness 0.12.

Another blunt Gasjet configuration with a flat frontal surface of the same circular cross section as the 0.12 blunt cone was computed at a Mach number of $M = 6.8$. The Mach number distribution and velocity vectors for the truncated blunt frontal nose are shown in Fig. 2.

A feature of particular bearing on flow stability is the inherent unsteady flow field (Fig. 3, right), which evolves as a result of the high Mach number flow field being confronted by the outflow immediately in front of the flat front surface. As discussed by Khalid and Juhany [17], the flow seems to be numerically unstable as the solution seems to converge followed by a breakdown of the flow field uniformity and deterioration of convergence. This behaviour seems to repeat near the convergence. This type of flow behaviour as discussed in reference [18, 19] is due to the carbuncle instability phenomenon.

It was observed in both computations and the shadowgraph that the outflow at the nose causes the stagnation region to be blown outwards in a spherical bubble shape pushing against the frontal shock. Note the presence of the supersonic bubble inside of the main shock. The flow region in between the main jet interface and the nozzle shock contains the slower expanded flow in both simulation and the experiment.

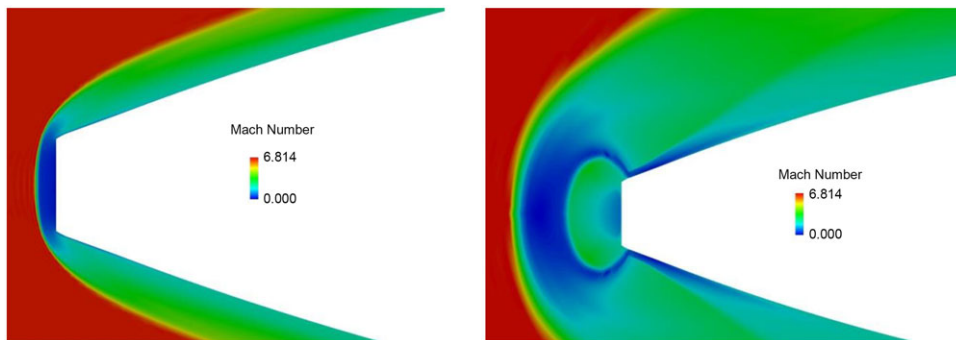


Figure 2. Mach number distribution past a solid blunt cone of (left) and with blowing (right).

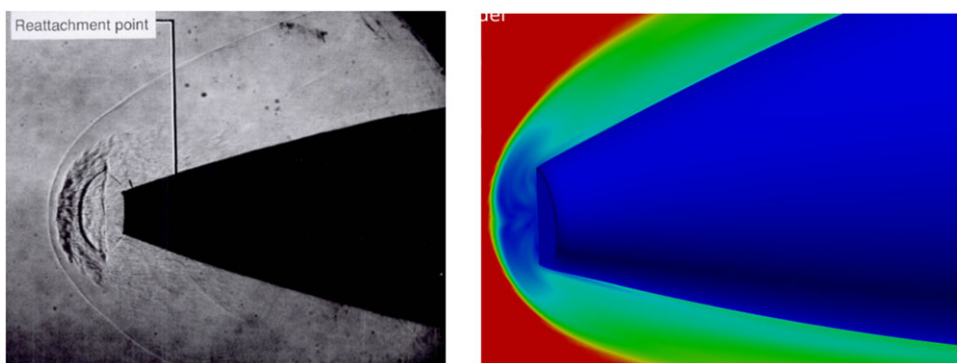


Figure 3. Gasjet experiment by Nowak (Ref. 8) $M = 6.8$, with a frontal blowing rate of, $\frac{\rho u_{local}}{\rho_{\infty} u_{\infty}} = 0.15$ (left). Note the unsteady flow near the leading edge (right).

The final set of results deal with a 0.32 bluntness cone with shoulder peripheral blowing just past the spherical nose. The flow field with and without the blowing from the shoulder jet of the Slatjet is shown in Fig. 4. It is clear from the viewgraph with shoulder blowing that the boundary layer is blown off from the surface with the strong peripheral jet from the shoulder.

The most important aspect of the present study was to be able to recover the steady pressure fields from above cases which are then in turn used in the following analysis to recover dynamic stability characteristics of blunt bodies. The pressure fields for the above blunt-nosed case bodies are shown in the following Fig. 5. While grid sensitivity study and the numerical error has been discussed in Khalid and Juhany [16, 17], it can be seen that the prediction especially on the straight portion of the model lies within 1–2% of the experiment.

The pressure distributions as computed on the blunt models showed satisfactory agreement with the measurements on the straight portion away from the blunt nose. The comparison for the blunt region was difficult, as no measurements had been recorded for this region.

3.0 Analytic approach to dynamic stability from steady flow field

The analytic approach relies on being able to obtain of a reliable pressure flow field and then using the classic shock expansion approach to perturb this solution. The angular displacement of a typical streamline near the surface of the body can be evaluated in terms of the pitch rate, the body half-angle and the flow velocity. The steady pressure distribution in all cases as discussed in previous discussion

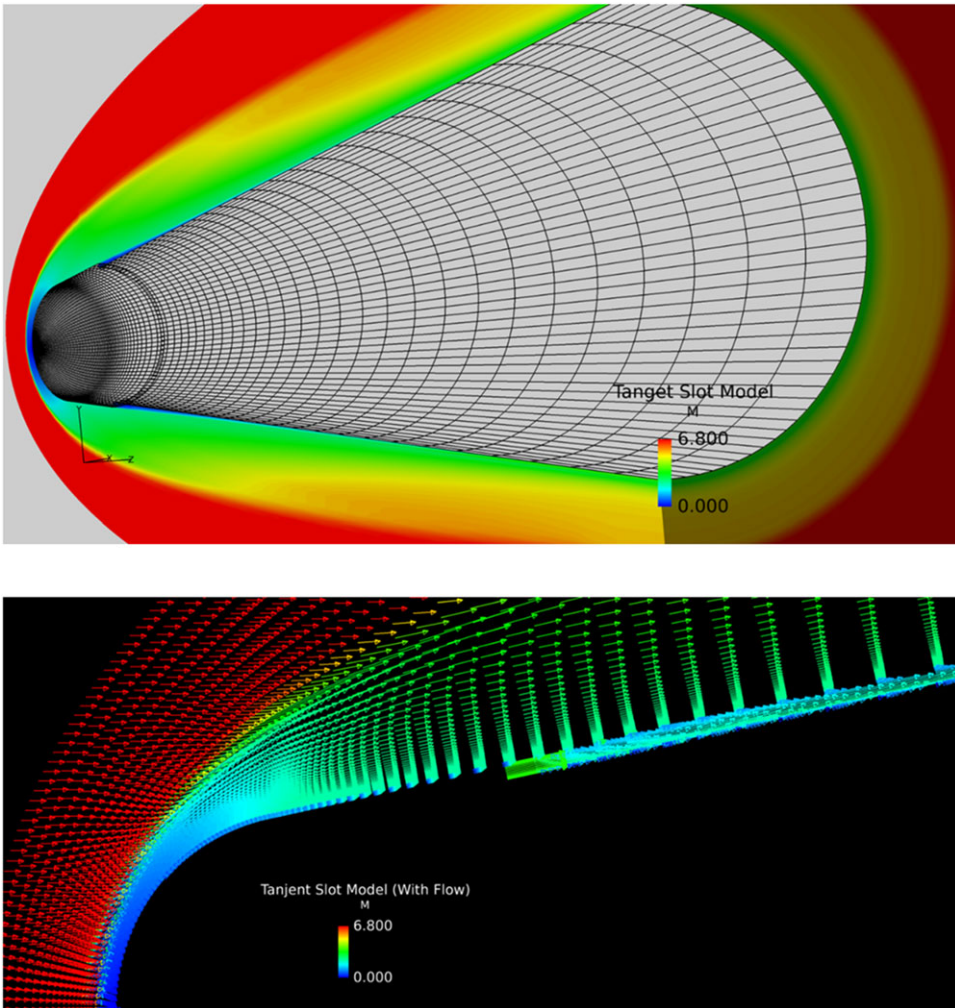


Figure 4. Slatjet solid model (top) and with shoulder blowing (bottom), blowing rate $= \frac{\rho u_{local}}{\rho_{\infty} u_{\infty}} = 0.15$.

was used from existing results on heat alleviation study [16, 17] on blunt conical bodies in hypersonic flow. The unsteady pressure at small angles of attack on an oscillating blunt body with or without blowing may be expressed in terms of the steady and unsteady component:

$$P_{b,s}(x, \alpha, t) = P_{b,s}(x, \alpha) + p'_{b,s}(x, \alpha) \tag{6}$$

Where, the subscripts *b* and *s* refer to either solid or frontal blowing condition and $p'_{b,s}$ refer to the instantaneous perturbation value as results of the body oscillations.

The unsteady pressure perturbation $p'_{b,s}$ may be evaluated from the shock expansion expression as developed by Eggers [20]. The shock expansion as used here will be drawn from Refs [21, 22] without entering too much detail. Hence:

$$p'_{b,s}(x, \alpha) = \frac{\rho V(x)^2}{\sqrt{(M_x^2 - 1)}} \Delta \epsilon_p \tag{7}$$

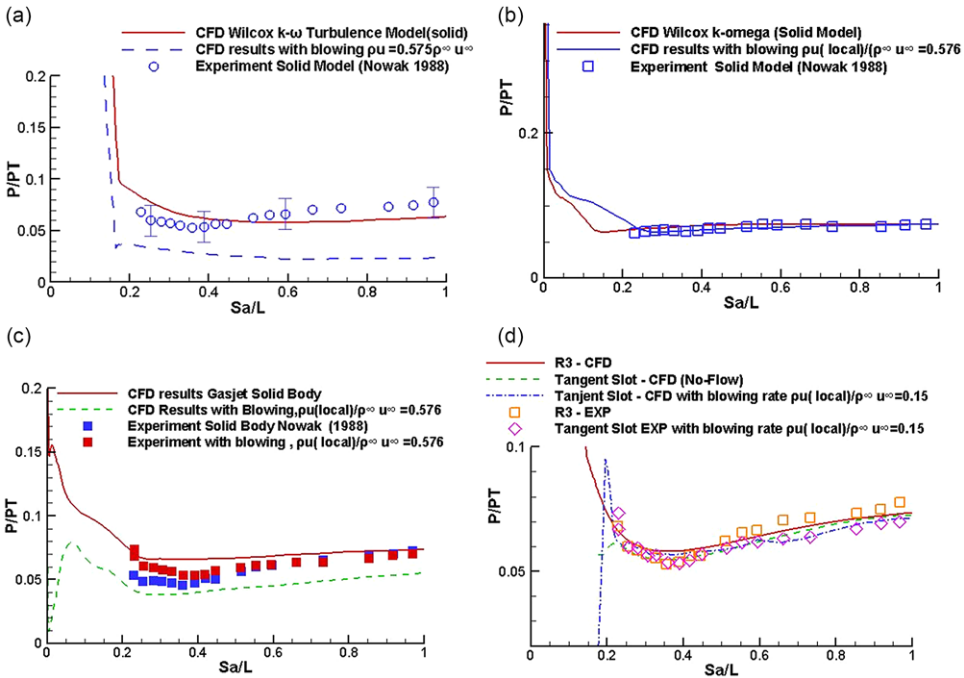


Figure 5. Pressure distributions on blunt-nosed bodies: R3 (a), R1 (b), Gasjet (c) and Slat-jet (d).

which gives,

$$\frac{P_{b,s}(x, \alpha, t)}{P_{b,s}(x, \alpha)} = 1 + \frac{\gamma M_x^2}{\sqrt{(M_x^2 - 1)}} \Delta \varepsilon_p(x) \tag{8}$$

Where $\Delta \varepsilon_p$ is the angular change of a particle from the body vertex to a station x along the body subject to a motion schedule involving plunging and or pitching motion. This angular change may be written in terms of the instantaneous height of the particle $h(x,t)$ and the expansion of the streamline along which it traverses. Thus following Scott [23],

$$\Delta \varepsilon_p(x) = \left| \tan^{-1} \left\{ \frac{dh(x, \tau(x))}{dx} \cdot \sin \varphi + \frac{dR(x)}{dx} \right\} \right| \tag{9}$$

This inclination angle $\Delta \varepsilon_p(x)$ of a path line projected on the surface of the body in purely pitching motion can be shown [16] as:

$$\Delta \varepsilon_p = (\theta_b(x) - \theta_0) + 2 \vartheta (\theta_b(x) - \theta_0) \sin \theta_0 \cos \theta_0 \sin \varphi - \frac{q}{V_\infty} \cos \theta_0 \sin \varphi \cdot \left\{ 2x + \tan \theta_0 \cdot \left[\int_0^x (\theta_b(x) - \theta_0) dx - (x - x_0) \cdot (\theta_b(x) - \theta_0) \right] + \frac{1}{\sqrt{M_\infty^2 - 1}} \cdot \left[\int_0^x (\theta_b(x) - \theta_0) dx - (x - x_0) \cdot (\theta_b(x) - \theta_0) \right] \right\} \tag{10}$$

where, θ_0 is the angle at the vertex and $\theta_b(x)$ is the inclination of the surface at the stations x . q is the body pitch rate, is the magnitude of the free stream velocity at the nose and M_∞ is the Mach number, which corresponds to the free stream velocity at the nose. For a conical body with constant surface slope ($\theta_b(x) = \theta_0$), the above expression simplifies to:

$$\Delta \varepsilon_p = -2x \frac{\cos \theta_0 \sin \varphi}{V_\infty} \tag{11}$$

and the effective angle-of-attack of the body pitching at q and instantaneous pitch angle ϑ is given by:

$$\alpha_e = \vartheta - \frac{q(x \sec \theta_0 + \theta_0)}{V_\infty} \tag{12}$$

The unsteady pressure can thus be written in terms of the instantaneous pressure perturbation and the effects from pitch rate and the effective angle-of-attack.

$$\frac{P_{b,s}(x, \alpha, t)}{P_\infty} = \frac{P_{b,s}(x, \alpha, t)}{P_{b,s}(x, \alpha)} \frac{P_{b,s}(x, \alpha)}{P_{x,\alpha=0}} \frac{P_{x,\alpha=0}}{P_{x,ref}} \frac{P_{x,ref}}{P_\infty} \tag{13}$$

The pressure distribution of a body at angle-of-attack with respect to the pressure at zero angle-of-attack is given by [24]

$$P_{,s}(x, \alpha) = P_{x,\alpha=0} - \eta \alpha_e \sin \varphi + \alpha_e^2 (D - \cos 2\varphi) \tag{14}$$

and where $\frac{P_{x,ref}}{P_\infty}$ represents the location on the spherical nose where the supersonic condition are first reached. This leads us to write the unsteady pressure coefficient as:

$$C_p = \frac{2}{\gamma M_\infty^2} \left\{ \frac{P_{b,s}(x, \alpha, t)}{P_\infty} \frac{P_{b,s}(x, \alpha, t)}{P_{b,s}(x, \alpha)} \frac{P_{b,s}(x, \alpha)}{P_{x,\alpha=0}} \frac{P_{x,\alpha=0}}{P_{x,ref}} \frac{P_{x,ref}}{P_\infty} - 1 \right\} \tag{15}$$

Static and pitching moment derivatives can now be obtained by obtaining $\frac{\partial C_p(b,s)}{\partial \alpha}$ and $\frac{\partial C_p(b,s)}{\partial q}$ and integrating the expression over the complete surface of the blunt body under solid and frontal blowing conditions, i.e.

$$Cm_\alpha = \frac{1}{Sl} \int_0^l \int_0^{2\pi} \frac{\partial C_p(b, s)}{\partial \alpha} R(x) l(x) \sin \varphi d\varphi dx \tag{16}$$

$$Cm_q = \frac{2V_\infty}{Sl} \int_0^l \int_0^{2\pi} \frac{\partial C_p(b, s)}{\partial q} R(x) l(x) \sin \varphi d\varphi dx \tag{17}$$

$l(x)$ is the moment arm $l = x \sec^2 \theta_0 - x_0$ and $R(x)$ is the local radius at station x . Pressure distribution for the blunt body under solid and blowing condition were successively introduced in the expression for the static and dynamic stability derivatives to obtain the stability characteristics. The above expression for Cm_q assumes that the $\dot{\alpha}$ effects in the expression $Cm_{\dot{\theta}}$ are very small and, in fact, $Cm_{\dot{\theta}} = Cm_q$.

4.0 Results

Static and dynamic derivatives were computed for the blunt configurations discussed above. For consistency, and also due to absence of measured data in the nose region, only the computed pressure fields were introduced into the expressions for static and dynamic derivatives. The static derivative Cm_α for the blunt cones is shown on the left side of Fig. 6.

The sharp cone result for the 12.5 deg half-angle (θ_0) is only introduced as a reference. The constant surface pressure from the conical relationships was $P_c/P_\infty = 3.94$, and the surface Mach number used was $M = 5.12$. It is clear that for axis position ahead of $X0 = 0.66$, the static stability decreases with increasing bluntness for the two blunt cones when compared to a corresponding sharp cone. The trend reverses after $X0 = 0.66$. It was learnt that the frontal blowing has no noticeable effect on the static stability. The blunt cones do, however, show that bluntness causes a consistent decrease in dynamic stability

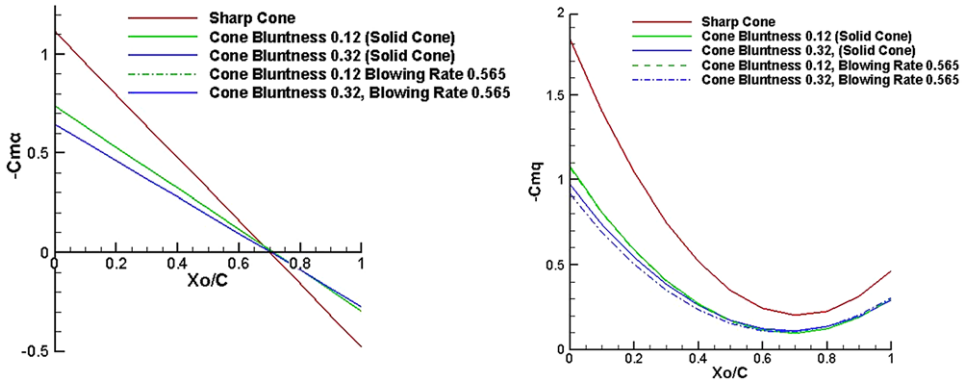


Figure 6. Static stability derivative (left) and dynamic stability derivative versus X_0/C .

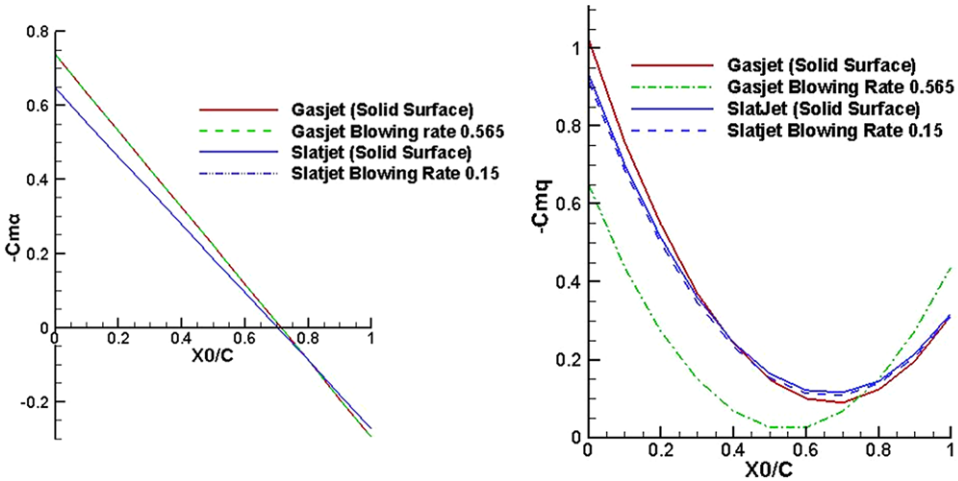


Figure 7. Static stability (left) and dynamic stability derivatives for the Gasjet and Slatjet versus X_0/C .

for all axis positions. It is also noted that, for cones of large bluntness, the blowing leads to deterioration in dynamic stability. For cones of smaller bluntness, the frontal blowing only has a relatively smaller surface area through which the outflow can be pumped, whereas the cones of larger bluntness will have a larger region through which the outflow can be effectuated, which leads to a relative larger interplay against the oncoming flow.

Examining the flow field physically, it appears that the flow impacting on the nose is opposed by the flow emerging from the blunt nose, which comprises the existing dynamic instability Cm_q between the flow and pitching cone. Increasing the bluntness leads to increasing interference between the flow and the underlying oscillating flow. This is certainly borne out by the fact that cones with larger bluntness experience incrementally more deterioration in dynamic stability. Since the effective angle-of-attack, $\alpha_e = \vartheta - \frac{q(x \sec \theta_0 + \theta_0)}{V_{\infty}}$ is not too adversely affected by the efflux from the blunt nose, the static stability Cm_{α} remains unaffected by blowing.

The static and dynamic derivative response against axis of oscillation position X_0/C for the Gasjet and the Slatjet are shown in Fig. 7. Once again the static stability derivative Cm_{α} , although shows a loss in stability with increased level of bluntness whether for the Gasjet or the Slatjet, yet the blowing does not cause any noticeable difference to the static stability. The dynamic stability derivative Cm_q , however,

is affected by the bluntness as well as by the blowing. The Gasjet, which is equipped with a flat surface to incorporate appropriate blowing, is most effective for creating a cooling bubble in front of the blunt nose. This cooling bubble produces a virtual bluntness which causes a depreciation of dynamic stability. Thus cooling in front leads to a decrease in dynamic stability derivative Cm_q when compared to the solid Gasjet body. The Slatjet experiment had used a small value of blowing $\frac{\rho u_{local}}{\rho_{\infty} u_{\infty}} = 0.15$ from the peripheral shoulder, which when applied at the aft conical surface of the Slatjet, may make a difference to the underlying heating rate, but it makes little difference to the dynamic stability derivative.

Once again, interpreting the flow physically, the model with larger efflux against the on-coming flow experiences larger adverse effect from blowing. The Gasjet model with a notably large blowing frontal area opposing the incoming flow and supporting a spherical flow bubble experiences the largest drop in dynamic stability for almost all axis locations upstream of $X0/C = 0.8$. Beyond $X0/C$ the bluntness and blowing effects are reduced as additional mass flow gives rise to body thickness effects showing some increase in dynamic stability. The slatjet, introduced tangentially into the flow field past the blunt surface region does not interfere as much with the incoming flow and the underlying blunt body. The slatjet may help with heat alleviation but does not adversely affect the dynamic stability. The static stability as alluded to earlier, depends directly upon the instantaneous angle-of-attack and is not affected by the pitching conditions q or $\dot{\vartheta}$.

5.0 Conclusion

The present analytic modeling shows that the static stability derivative is not too adversely by blowing as the expression for Cm_{α} is driven largely by the steady pressure distribution and not by the pitching conditions q or $\dot{\vartheta}$. The dynamic stability appears to depreciate with both bluntness and blowing rate. Cones of smaller bluntness cannot be equipped to force excessive outflow from small blunt regions and thus their stability is not affected by blowing.

Dynamic stability of cones with sharp square-edged frontal bluntness equipped with blowing suffer more than the cones with tangential shoulder blowing. This is because the sharp edge in front traps a larger region of slower air bubble than simple rounded nose, which smoothly diverts the air downstream. The incoming flow is disturbed with larger bluntness and blowing leading to depreciation of Cm_q .

Competing interests. The authors declare none.

References

- [1] Rie, H., Linkiewicz, E.A. and Bosworth, F.D., Hypersonic Dynamic Stability, Part III, Unsteady flow Field program, FDL-TDR-64-149; January 1967, Air Force Flight Dynamics Lab, Wright-Patterson Air Force Base, USA.
- [2] Shueler, C.J., Ward, L.K., and Hodapp, Jr., A.E., Techniques for Measurement of Dynamic Stability Derivatives in Ground Testing Facilities, AGARD 121, October, 1967.
- [3] Dynamic stability parameters, AGARD Conference Proceedings, AGARD CP-235.
- [4] Khalid, M. and Juhany, A.K. An expression for the dynamic stability of slender elliptic wings in hypersonic flow, *Aeronaut. J.*, 2014.
- [5] Khalid, M. and Juhany, A. Dynamic stability of wave riders, *J. Aircraft Eng. Aerospace Technol.*, 2016. doi: [10.1108/AEAT-09-2015-0218.R2](https://doi.org/10.1108/AEAT-09-2015-0218.R2)
- [6] Nowak J.R. Gasjet and tangent slot cooling film tests of a 12.5° . Cone at $M = 6.7$, NASA Technical Paper 27866, 1988.
- [7] Tissera, S., Drikakis, D. and Birch, T. Computational fluid dynamics methods for hypersonic flow around blunted-cone-cylinder-flare, *J. Spacecraft Rockets*, 2010, **47**, (4), pp 563–570.
- [8] Panaras, A.G. and Drikakis, D. High-speed unsteady flows around spiked-blunt bodies, *J. Fluid Mech.*, 2009, **632**, pp 69–96.
- [9] Narayan, A., Suramanian, N., Kumar, R. and Singh, T. Control of aerodynamics drag and heating of nose cones through taper ratios, *Progress Comput. Fluid Dyn. Int. J.*, 2020, **20**, (2), pp 105–123.
- [10] Watanabe, Y. et al. Aerodynamic characteristics of breathing blunt nose configuration at hypersonic speeds, *Proceedings of the Institution of Mechanical Engineers, Part G: Journal of Aerospace Engineering*, 2017, **231**, (5), pp 840–858.
- [11] Vinokur, M. Conservation equations of Gas Dynamics in curvilinear coordinate system, *J. Comput. Phys.*, 1974, **14**, pp 105–125.

- [12] Beam, R. and Warming, R.F. An implicit finite difference algorithm for hyperbolic systems in conservation law form, *J. Comput. Phys.*, 1976, **22**, (1), pp 87–110.
- [13] Pulliam, T. and Chaussee D.S., A diagonal form of an implicit approximate-factorization algorithm, *J. Comput. Phys.*, 1981, **39**, (2), pp 347–363.
- [14] Grundmann, R., *Aerothermodynamik*, Springer Verlag, 1, 2000.
- [15] Gordon, S. and McBride, B.J. Computer program for calculation of complex chemical equilibrium compositions and applications, Tech Rep, National Aeronautics and Space Administration, Office of Management, Sciatic and Technical Information Program, 1994.
- [16] Khalid, M. and Juhany, A.K., Heat alleviation studies on hypersonic vehicles, *Aeronaut. J. Aero J.*, 2018, **122**, (1257), pp 1673–1696.
- [17] Khalid, M. and Juhany, A.K. Innovative means of surface blowing towards heat alleviation for hypersonic flows, *J. Aerospace Eng.*, 2019, **2019**, p 18.
- [18] Garicano-Mena J, Lani A, Deconinck H. An energy-dissipative remedy against carbuncle: Application to hypersonic flows around blunt bodies, *Comput. Fluids*, 2016, **133**, pp 43–54.
- [19] Ismail, F and Roe, P.L. Affordable, entropy-consistent Euler flux functions II: entropy production at shocks, *J. Comput. Phys.*, 2009, **228**, (15, 20), pp 5410–5436.
- [20] Eggers, A.J. On the calculation of flow about objects travelling at high supersonic speeds, NACA TN 2811, 1952.
- [21] Khalid, M. and East, R.A. Stability derivatives of blunt cones at high Mach Numbers, *Aeronaut. Q.*, 1979, **30**, pp 559–590.
- [22] Khalid, M. and East, R.A. High mach number dynamic stability of pointed cones at angles of attack, *AIAA J.*, 1980, **18**, pp 1263–1284.
- [23] Scott, C.J. A theoretical and experimental determination of the pitching derivatives of the pitching stability derivatives of cones in hypersonic flow, MSc Thesis, AASU Report No. 67, University of Southampton, UK.
- [24] Krasnov, N.V. *Aerodynamics of Bodies of Revolution*, Edited and Annotated by Dean N Morris, American Elsevier Publishing Company, 1970, New York.